

# Measuring ac Magnetic Susceptibility at Low Frequencies with a Torsion Pendulum for Gravitational-Wave Detection

Jia-Hao Xu (徐家豪)<sup>1</sup>, Qi Liu (刘祺)<sup>1,\*</sup>, Xue Luo (罗雪)<sup>1</sup>, Lin Zhu (郑琳)<sup>1,2,†</sup>, Hui-Hui Zhao (赵慧慧)<sup>2</sup>, Qing-Lan Wang (王晴岚)<sup>3</sup>, Shan-Qing Yang (杨山清)<sup>1</sup>, and Jun Luo (罗俊)<sup>1</sup>

<sup>1</sup> MOE Key Laboratory of TianQin Mission, TianQin Research Center for Gravitational Physics & School of Physics and Astronomy, Frontiers Science Center for TianQin, Gravitational Wave Research Center of CNSA, Sun Yat-sen University (Zhuhai Campus), Zhuhai 519082, People's Republic of China

<sup>2</sup> MOE Key Laboratory of Fundamental Physical Quantities Measurement, Hubei Key Laboratory of Gravitation and Quantum Physics, PGMF and School of Physics, Huazhong University of Science and Technology, Wuhan 430074, People's Republic of China

<sup>3</sup> School of Mathematics, Physics and Optoelectronic Engineering, Hubei University of Automotive Technology, Shiyan 442002, People's Republic of China



(Received 7 March 2022; revised 4 July 2022; accepted 26 August 2022; published 5 October 2022)

The measurement of ac susceptibility  $\chi(\omega)$  down to 0.1 mHz of test masses is vital for TianQin, a Chinese space-based gravitational-wave detection mission, since the magnetic induced disturbing force is one of the main contributors to residual acceleration noise of test masses. Here we report a method based on a torsion pendulum with dual magnetic field modulation to measure  $\chi(\omega)$  of centimeter-scale test mass from 50  $\mu$ Hz to 80 Hz. The measurement resolution can reach a level of  $10^{-8}$ , meeting the requirements of TianQin. Meanwhile, this method also provides an important ground-validation approach for the down-converted effects [Phys. Rev. Lett. 120, 061101 (2018)] from ac magnetic fields, potentially reducing the risk of failure in space.

DOI: 10.1103/PhysRevApplied.18.044010

## I. INTRODUCTION

Space-based gravitational-wave (GW) detection provides a unique tool for testing gravity, and opens a ground-breaking low-frequency observation window below 1 Hz for astronomy and cosmology [1–3]. TianQin, which consists of three Earth-orbiting satellites in a nearly equilateral triangle formation, was proposed to detect GWs at a frequency band of  $10^{-4}$  to 1 Hz in space [4]. In each satellite, isolated metal test masses act as a free-falling reference. They are expected to orbit along the geodesic curve with a residual acceleration noise below  $1 \times 10^{-15} \text{ m s}^{-2} \text{ Hz}^{-1/2}$  from  $10^{-4}$  to 1 Hz [5]. The requirement of the residual acceleration is stricter than LISA, since the arm length of TianQin is an order of magnitude shorter than that of LISA. On the other hand, TianQin satellites are much closer to the Earth and the Moon, and the test masses would subject to a stronger influence of the magnetic fields from the Earth and the Moon [6]. Therefore, the magnetic noise would be more a serious issue for TianQin than for LISA. The magnetically induced force is expected to

contribute to 24% of the residual acceleration noise budget in TianQin, and it should be treated cautiously [4,6,7]. The induced magnetic force can be described by the coupling of remnant magnetic dipole  $\vec{m}_r$  and susceptibility  $\chi$  of a test mass to the fluctuations of ambient magnetic field [8,9]. In TianQin, the test masses are made of Au-Pt alloy and the cleanliness of  $\chi$  should be lower than  $1 \times 10^{-6}$  [6,7]. Consequently, a high-resolution measurement of  $\chi$  at a level of  $1 \times 10^{-7}$  on the ground is unavoidable. Furthermore,  $\chi$  is not a constant but a frequency-dependent function  $\chi(\omega) = \chi_0 + i\chi_e(\omega)$ , which requires one to measure  $\chi(\omega)$  at the relevant frequency band of GW detection missions [10]. For TianQin, the focus is to detect the GW signal within the low-frequency band; thus, the measured frequency band of susceptibility  $\chi(\omega)$  of the test mass should be at the sub-millihertz range. In addition, recent LISA Pathfinder (LPF) experimental results have pointed out that the relatively high-frequency ( $>10$  Hz) magnetic fields “down-converting” into the LPF band by the  $\nabla B^2$  dependence of the magnetic force are also a noise source coupling to the test mass [11]. Therefore measurements of the susceptibility  $\chi(\omega)$  up to higher frequencies are also highly necessary for noise estimation. Hence, it is essential to develop an experimental method to determine  $\chi(\omega)$  with

\*liuq239@sysu.edu.cn

†zhulin36@hust.edu.cn

a resolution at a level of  $1 \times 10^{-7}$  within the frequency band from  $10^{-4}$  Hz to a few hundred hertz. It should be noted that ac susceptibility is a quantity defined under a uniform ac magnetic field [12,13]; therefore, the magnetic force induced by a complex magnetic field cannot be accurately calculated using the concept of ac susceptibility. However, the measurement of ac susceptibility still provides a direct and general characterization of the magnetic properties of a test mass under relatively uniform time-varying magnetic fields. It is an important quantity for the valuable approximate estimation of the magnetic effect [8,14].

Trougnou *et al.* employed induced bridges to test the ac susceptibility of the test mass used in LPF from 1 to 600 Hz, but the sensitivity band is limited above approximately 1 Hz [15]. Hueller *et al.* proposed a measurement scheme of susceptibility of centimeter-scale test mass by a precision torsion pendulum with satisfactory resolution, whereas the measurable frequency of susceptibility was not discussed [9]. The ac susceptibility of the test mass used in LPF has been measured by LPF in-flight operations, and the measured frequency is less than 30 mHz [14]. Also, conventional devices or methods such as superconducting quantum interference device (SQUID) magnetometers cannot meet the present requirements due to the measurable frequency limitation or the resolution or the sample size [16]. There is no existing way to determine the ac susceptibility of a centimeter-scale test mass within the TianQin required measurement resolution and frequency band.

## II. METHOD AND INSTRUMENT

In the measurement of ac susceptibility with a relatively homogeneous monochromatic magnetic field, the magnetic induced force applying to the test mass can be approximately written as [17]

$$\vec{F} = \nabla [(\vec{m}_r + \chi(\omega)V\mu_0^{-1}\vec{B}(\omega)) \cdot \vec{B}(\omega)], \quad (1)$$

where  $\vec{m}_r$  is the constant intrinsic remanent magnetic dipole,  $\mu_0$  is the magnetic permeability,  $V$  is the volume of the test mass,  $\vec{B}(\omega)$  is the ambient magnetic field, and  $\chi(\omega)V\mu_0^{-1}\vec{B}(\omega)$  is the induced magnetic moment. In some previous classical methods based on a torsion pendulum [18], a single-frequency magnetic field  $\vec{B}(\omega)$  and its field gradient  $\nabla\vec{B}(\omega)$  were applied. Since the  $\chi(\omega)$ -related force depends on  $\nabla[\chi(\omega)\vec{B}^2(\omega)]$ , a single-frequency measured force at  $2\omega$  would be imposed on the torsion pendulum. As the sensitive bands of typical torsion pendulums responding to the measured force are limited within a narrow band ranging from  $10^{-4}$  to  $10^{-3}$  Hz [19], the measurable frequency band of  $\chi(\omega)$  of the test masses will be restricted below  $10^{-3}$  Hz.

In this paper, we present a measurement method of ac susceptibility using a sensitive torsion pendulum with dual

modulation of magnetic field. A specially designed magnetic field  $\vec{B}_s = \vec{B}_I + \vec{B}_F$  is applied to the test mass, where  $\vec{B}_I$  is a uniform magnetic field and  $\vec{B}_F$  is a synclastic uniform-gradient magnetic field. Both  $\vec{B}_I$  and  $\vec{B}_F$  are modulated with different frequencies  $\omega_I$  and  $\omega_F$ , respectively. If we apply  $|\vec{B}_I| \gg |\vec{B}_F| = 0$  and  $|\nabla\vec{B}_F| \gg |\nabla\vec{B}_I| = 0$  and we take the designed  $\vec{B}_s$  into Eq. (1), then the magnetic induced force can be written as

$$F(\omega_I \pm \omega_F) = \chi(\omega_I) \left[ \frac{B_I(\omega_I)}{2\mu_0} \nabla B_F(\omega_F) \right]. \quad (2)$$

It is noted that  $\chi$  is modulated at frequency  $\omega_I$  since  $|\vec{B}_F| = 0$  but the force signal is modulated at the sum and difference of  $\omega_I$  and  $\omega_F$ . It is beneficial to take advantage of these properties by selecting appropriate combination of  $\omega_I$  and  $\omega_F$ , and make sure the targeted force  $F(\omega_I \pm \omega_F)$  falls in the sensitive band of the torsion pendulum. Hence, by dual-frequency-modulation technology, the method can broaden the measurable frequency band and maintain high sensitivity of the devices with an extreme force resolution.

A schematic of the measuring device is shown in Fig. 1. The device is a two-stage torsion pendulum suspended by a 60-cm-long and 50-μm-diameter tungsten fiber. The pendulum body is constituted by a 22-cm-long aluminum crossbar, the 2-cm-side cubical-shaped copper (99.99% purity [20]) test mass, and its counterweight mass. The test mass and the counterweight mass are suspended with 300-μm-diameter tungsten fibers to each end of the bar.

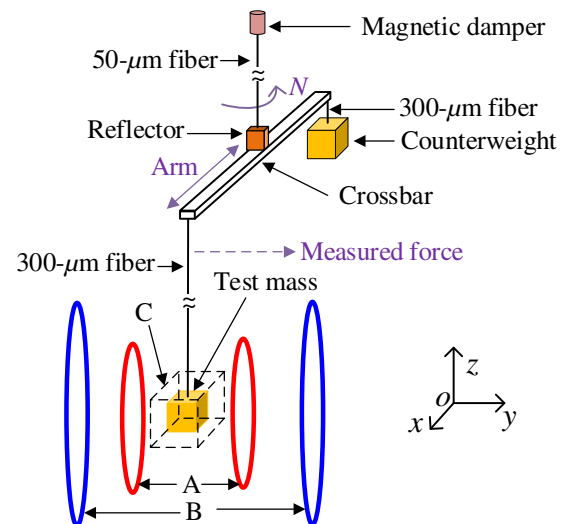


FIG. 1. Schematic diagram of the device. A, Helmholtz coils; B, constant-gradient Maxwell coils, the coils being coaxial; C, homogeneous area of magnetic field, and the cube test mass at the center of the area. The origin of the coordinates is at the center of the cube, and horizontal coordinates are parallel with the sides of the cube (the  $y$  axis is set along the axes of the coils and the  $z$  axis is set parallel to the 300-μm-diameter fiber).

A reflector used for optical readout of the pendulum rotational angle is located at the center of the bar. The external magnetic field generators include Helmholtz coils ( $H$ -coils, 20 cm in diameter, 490 turns) and constant-gradient Maxwell coils [21] ( $M$ -coils, 40 cm in diameter, 270 turns) with designed 1% of the  $H$ -coil and 0.5% of the  $M$ -coil field uniformity in a cubical space (3-cm side length). The test mass can entirely be located inside this cubical space. The  $H$ -coils and  $M$ -coils are used to produce separately the uniform induced magnetic field  $B_I$  and the uniform magnetic field gradient  $B_F$ . As Fig. 1 shows, the dominant components of fields are along the  $y$  axis, i.e.,  $|\vec{B}_I| \simeq B_{Iy}$  and  $|\nabla \vec{B}_F| \simeq \partial B_{Fy} / \partial y$ . The entire device is installed in a vacuum chamber maintained at a pressure of  $10^{-5}$  Pa during the experiment. The pendulum body twist  $\theta(t)$  is monitored by an autocollimator that reflects the light off the reflector continuously every 40 ms. The natural resonant period of the pendulum, with calculated moment of inertia  $I = 1.491 \times 10^{-3}$  kg m<sup>2</sup>, is 625.2 s.

With stimulating currents into  $H$ -coils and  $M$ -coils at nearby frequencies  $\omega_I$  and  $\omega_F$  respectively, namely  $B_I(t) = B_I \cos(\omega_I t)$  and  $B_F(t) = B_F \cos(\omega_F t)$ . For simplification of data analysis, the initial phases of the two fields are set to zero. According to Eq. (2), the pendulum senses two susceptibility-related torques, expressed as

$$\begin{aligned} N_\chi(t) &= bF(\omega_I \pm \omega_F) \\ &= |\chi(\omega_I)|P_\chi \cos[(\omega_I \pm \omega_F)t + \varphi(\omega_I)], \end{aligned} \quad (3)$$

where  $b$  is the crossbar arm length of the pendulum,  $|\chi(\omega_I)| = \sqrt{(\chi')^2 + (\chi'')^2}$  and  $\varphi(\omega_I) = \tan^{-1}(\chi''/\chi')$  are the modulus and the phase (or lag) of  $\chi(\omega_I) = \chi'(\omega_I) + i\chi''(\omega_I)$ , respectively, and  $P_\chi = b(2\mu_0)^{-1}B_{Iy} \cdot \partial B_{Fy} / \partial y$  is the parameter determined by the applied fields. The ac susceptibility  $\chi(\omega_I)$  is determined from the amplitude and the initial phase of the time series  $N_\chi(t)$ .

### III. DATA ANALYSIS

The  $N(t)$  is estimated from monitored data of the pendulum twist  $\theta(t)$  through the torsion pendulum equation of motion:  $N(t) = I\ddot{\theta}(t) + \beta\dot{\theta}(t) + k\theta(t)$ , with known  $I$ , elastic constant  $k = 1.50 \times 10^{-7}$  rad/N m of the measured fiber, and internal damping coefficient  $\beta = 5.76 \times 10^{-9}$ . The derivatives  $\ddot{\theta}(t)$  and  $\dot{\theta}(t)$  are calculated from a fitted sliding second order to five adjoining data points with a minimum chi-square value [22]. This processing can eliminate the natural resonant signal, linear drift, and avoid subtle errors. The time series  $N(t)$  are accumulated continuously, and cut into segments with appropriate duration (typically 3000 s). Data from each cut are analyzed by

fitting the torque  $N(t)$  as a function of  $t$ :

$$N(t) = \sum_{i=1}^4 N(\omega_i) \cos(\omega_i t + \phi_i), \quad (4)$$

where  $N(\omega_i)$  and  $\phi_i$  are the amplitude and initial phase of the sinusoidal signals at different  $\omega_i$  [23,24]. The estimations of  $N(\omega_i)$  and  $\phi_i$  are the statistical average of fitted data from each cut. Then, the  $N_\chi(t)$  can be extracted, and later the modulus and phase of ac susceptibility are estimated based on Eq. (3).

### IV. RESULTS AND DISCUSSION

To measure  $\chi(\omega_I)$  of the cubical-shaped copper at the sub-millihertz level, both coil frequencies can be set inside the sensitive band of the pendulum. For instance, we apply a series of combined currents into the  $H$ -coils and  $M$ -coils at  $\omega_I = 0.5$  mHz and  $\omega_F = 0.9$  mHz separately. When applying a 15-mA current into both coils, the power spectral density (PSD) of the torque is shown in the top panel of Fig. 2. There are four notable relevant signals, two of which are at 0.4 and 1.4 mHz, corresponding to the measured  $N(\omega_I - \omega_F)$  and  $N(\omega_I + \omega_F)$ , respectively. The other two are nonrelevant remanent magnetization-related signals at 0.5 and 0.9 mHz, respectively. The maximum torque sensitivity of the torsion pendulum is about  $2 \times 10^{-12}$  N m/Hz<sup>1/2</sup> around the frequency of each target signal. Taking the typical value of  $P_\chi = 1 \times 10^{-6}$  N m (30-mA currents are applied to both

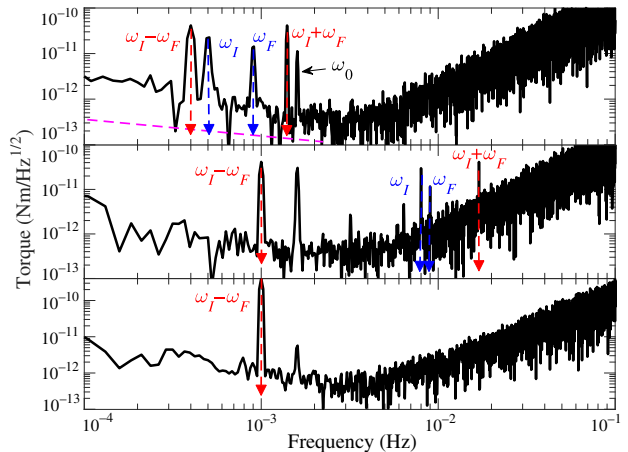


FIG. 2. Top: In black, the PSD of the pendulum torque from the measurement of  $\chi(\omega = 0.5$  mHz). The pink dashed line shows the thermal noise limit, with a quality factor  $Q \approx 2700$ . Spectrum of a 30-h measurement is calculated with a time-domain filtering [25]. The natural resonance frequency approximates to  $\omega_0 = 1.6$  mHz. Middle: The PSD of the pendulum torque from the measurement of  $\chi(\omega = 8$  mHz) with a 15-h duration. Bottom: The PSD of the pendulum torque from the measurement of  $\chi(\omega = 10$  Hz) with a 15-h duration.

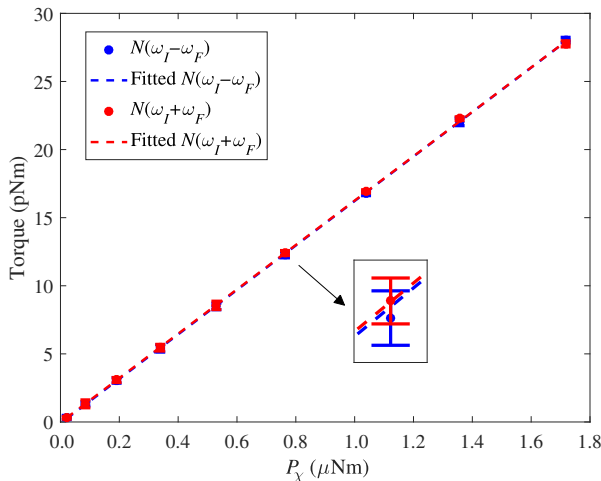


FIG. 3. The measured torques  $N(\omega_I - \omega_F)$  (blue circles) and  $N(\omega_I + \omega_F)$  (red circles) in different  $P_\chi$  sets. The blue and red dotted lines are the fitted lines of  $N(\omega_I - \omega_F)$  and  $N(\omega_I + \omega_F)$ , respectively. The slopes of the lines represent the modulus of the ac susceptibility.

of the coils), and applying a 3-h integration time, this sensitivity performance yields an expected susceptibility resolution of  $|\Delta\chi| \simeq 2 \times 10^{-8}$ , well below the TianQin requirements.

We measure the torques  $N(\omega_I - \omega_F)$  and  $N(\omega_I + \omega_F)$  under nine  $P_\chi$  sets by changing the injection currents of the coils. The results for the torques are shown in Fig. 3. The errors of  $\chi(\omega_I)$  are fully evaluated in Table I. The constant systematic relative error is about 1.44% mainly due to the imperfect uniformity of the fields. The very small statistical relative error of 0.1% is calculated in data processing of  $N(\omega_I \pm \omega_F)$ . The susceptibility is estimated by the linear fit of  $N(\omega_I - \omega_F)$  or  $N(\omega_I + \omega_F)$  with  $P_\chi$ , and the estimated susceptibilities at 0.5 mHz are  $(1.664 \pm 0.024(\text{syst}) \pm 0.002(\text{stat})) \times 10^{-5}$  and  $(1.662 \pm 0.024(\text{syst}) \pm 0.002(\text{stat})) \times 10^{-5}$ , respectively. They are in excellent agreement with each other. This shows the coincidence and reliability of our experiment. It also

indicates that either signal  $N(\omega_I - \omega_F)$  or  $N(\omega_I + \omega_F)$  can give the same measurement results for  $\chi(\omega_I)$ .

The middle panel of Fig. 2 demonstrates the measurement of  $\chi(\omega)$  at a slightly higher frequency. We implement a measurement of  $\chi(\omega_I = 8 \text{ mHz})$  by applying currents into the  $H$ -coils and  $M$ -coils at 8 and 9 mHz separately. The difference-frequency torque signal  $N(\omega_I - \omega_F)$  is located at 1 mHz where the torsion pendulum has the most sensitive resolution. When the sum-frequency torque signal  $N(\omega_I + \omega_F)$  is modulated at 17 mHz, the torque sensitivity is about one order of magnitude worse. The susceptibilities at 8 mHz estimated from  $N(1 \text{ mHz})$  and  $N(17 \text{ mHz})$  are  $(5.18 \pm 0.08(\text{syst}) \pm 0.10(\text{stat})) \times 10^{-5}$  and  $(5.25 \pm 0.08(\text{syst}) \pm 0.95(\text{stat})) \times 10^{-5}$ , respectively. Since both the torques  $N(\omega_I - \omega_F)$  and  $N(\omega_I + \omega_F)$  give the same information for  $\chi(\omega_I)$ , we can choose  $N(\omega_I - \omega_F)$  to calculate the value of  $\chi(\omega_I = 8 \text{ mHz})$  with much higher precision.

The frequency of the  $\chi(\omega_I)$  measurement can be set far higher than that of the typical torsion pendulum. For instance,  $\omega_I$  and  $\omega_F$  are set to be 10 and 10.001 Hz, respectively. The PSD of the sensed torque of the torsion pendulum is shown in the bottom panel of Fig. 2. There is only one measurable signal, i.e.,  $N(\omega_I - \omega_F)$  located at 1 mHz, while the other three torques around 10 and 20 Hz are out of the sensitivity band of the torsion pendulum and cannot be seen in the PSD. The estimated susceptibility at 10 Hz is  $(5.59 \pm 0.08(\text{syst}) \pm 0.11(\text{stat})) \times 10^{-2}$ . This measurement also experimentally proves the “down-converting” effect proposed in Ref. [11], i.e., the magnetic field and related gradient field variation around 10 Hz can induce a force acting on the test mass at lower frequency of 1 mHz. Thus, our torsion pendulum can also serve as a test bench for this effect, and allow full estimation of the residual acceleration noise  $a(\Omega)$  in space-based GW detection missions by knowledge of  $\chi(\omega)$  and the corresponding correlation function of  $B(\omega)$  with  $\nabla B(\omega)$ . Then  $a(\Omega)$  can be given by

$$a(\Omega) = \frac{1}{m} \int_0^\infty \chi(\omega) V \mu_0^{-1} B(\omega) \nabla B(\omega + \Omega) d\omega, \quad (5)$$

where  $0.1 \text{ mHz} < \Omega < 1 \text{ Hz}$  is the GW detection band and  $m$  is the mass of the test mass. In practice, the upper limit of the integral should be taken as high as 100 Hz where the energy of ac magnetic field  $B(\omega)$  of space is mainly distributed [26]. Since the measurement band of the existing on-board magnetometer sensor is below 1 Hz, the matched designs of high-frequency magnetic field sensor are required [17,27].

We sweep  $\omega_I$  from 50  $\mu\text{Hz}$  to 80 Hz (the upper frequency is limited by the performance of our current source), and the results for  $|\chi(\omega)|$  and  $\varphi(\omega)$  of the copper sample are shown in Figs. 4 and 5, respectively. The value of  $|\chi(\omega)|$  below  $10^{-3}$  Hz is nearly constant and

TABLE I. One  $\sigma$  uncertainty budget (in units of  $10^{-3}$ ).

Error sources	$\Delta\chi/\chi$
Uniformity of $B_{ly}$	12
Uniformity of $\partial B_{Fy}/\partial y$	8
Geomagnetic field	<0.1 (corrected)
Moment of inertia	<0.3
Force arm $b$	<0.1
Combined systemic relative error	14.4
Fluctuation of applied fields	<0.1
Fluctuation of damping coefficient $\beta$	<0.05
Combined statistical of torque $N$	0.1
Total	14.4

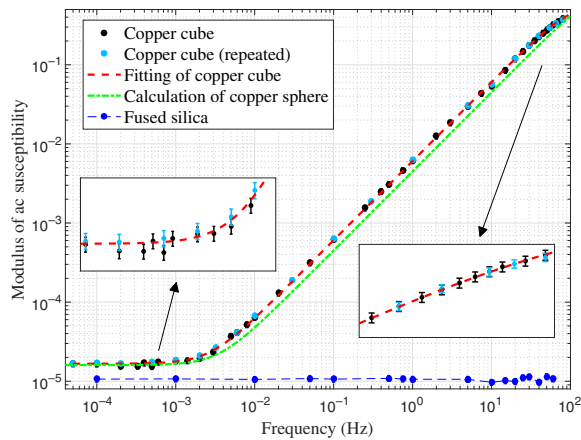


FIG. 4. The black circles are measured modulus  $|\chi(\omega)|$  of the ac susceptibility of the copper cube at different frequencies from data in November 2021. The light-blue points are repeat-measured modulus  $|\chi(\omega)|$  of the same copper cube from data in June 2022. The red dotted curve is the fitted model from Eq. (6). The green dotted curve is the calculated modulus of ac susceptibility of a 2-cm-diameter sphere with measured  $\chi_0$ . The blue circles are the measured values of the modulus of ac susceptibility of fused silica for comparison.

then increases rapidly. The frequency dependence of the ac susceptibility was modeled in Refs. [8,14]. Based on that previous model, we fit the data using the nonlinear least-squares method:

$$\chi(\omega) = \chi_0 + A_0 \left( \frac{\omega^2 \tau_e^2}{1 + \omega^2 \tau_e^2} + i \frac{\omega \tau_e}{1 + \omega^2 \tau_e^2} \right), \quad (6)$$

with fitted  $\chi_0 = -(1.66 \pm 0.08) \times 10^{-5}$  being the approximate constant susceptibility at frequency close to zero,

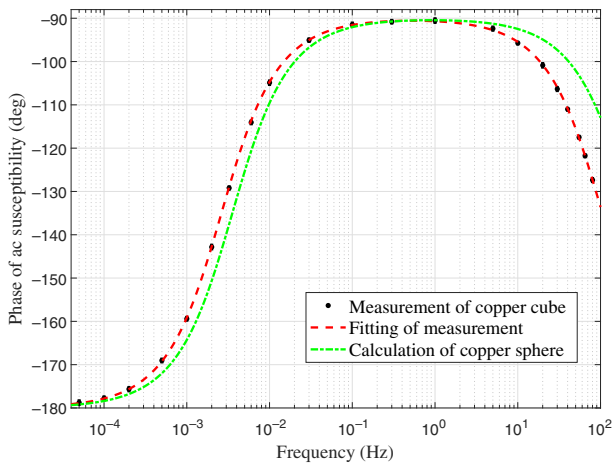


FIG. 5. The black circles are measured phase  $\varphi(\omega)$  of the ac susceptibility of the copper cube at different frequencies from data in June 2022. The red dotted curve is the fitted model from Eq. (6). The green dotted curve is the calculated phase of ac susceptibility of a 2-cm-diameter sphere with measured  $\chi_0$ .

$\tau_e = 1/(2\pi \times (105 \pm 4))$  the roll-off frequency, and the fitted value  $A_0 = -(0.64 \pm 0.02)$ . The results clearly show that there are two different physical behaviors of magnetization of copper in the frequency domain. At the ultra-low-frequency band below 2 mHz, the magnetic dynamics can be characterized by the quasistatic process of the sample inner magnetization [13]. When the frequency is above 2 mHz, the ac susceptibility mainly originates from the eddy currents on the sample surface induced by its ambient ac magnetic field [28].

We repeat the whole experiment but replacing the copper sample with fused silica of the same shape [20], and find the susceptibility is frequency independent within our test resolution. The ac susceptibility of the fused silica at the millihertz level is  $(1.061 \pm 0.015\text{ (syst)} \pm 0.008\text{ (stat)}) \times 10^{-5}$ , which is coincident with the measured value in Ref. [29], also shown in Fig. 4. There is no free charge inside the fused silica, and thus no eddy current can be induced by the ac magnetic field.

We calculate the ac susceptibility of a 2-cm-diameter copper sphere using the method reported in Ref. [12]. The calculated  $\chi(\omega)$  and  $\varphi(\omega)$  of the copper sphere are also shown in Figs. 4 and 5, respectively. It can be seen that the calculated results are in good agreement with the measured results, which indicates that our measured methods are reliable and results are correct.

The  $\chi(\omega)$  of Au-Pt alloy test mass used for space-based GW detection may have properties similar to those of copper. The parameters in Eq. (6) are dependent not only on the material of the test mass but also on other properties such as the surface conductivity, size, shape, and so on [30]. The actual Au-Pt alloy test mass ac susceptibility should be carefully tested before launch. Since the side length of the Au-Pt cube is about two times larger than that of the present copper sample, a modified torsion pendulum system that can hold a test mass of about 2 kg is under construction. Other improvements of the devices are also under investigation, including optimizing the coils for generating more uniform magnetic fields, and using a high-frequency drive circuit for measurement frequency reaching to kilohertz.

## V. SUMMARY

In summary, we measure the ac susceptibility  $\chi(\omega)$  of a copper cube at the frequency band ranging from 50  $\mu$ Hz to 80 Hz with a  $10^{-8}$  resolution level, which can meet the requirements of TianQin. The measurement method can be used to characterize the magnetic properties of a Au-Pt alloy test mass, and thus put forward constraints for the design of TianQin satellites to ensure the magnetic field generated by other equipment will not exceed the requirements. Besides the application in GW detection, measurements of susceptibility at low frequency could be used to investigate fundamental dynamic physical

mechanisms such as magnetic phase transitions [31], magnetic relaxations [32], Rayleigh hysteresis [33], and random interactions of magnetic spins [34]. We believe that the measurement method has great potential to contribute in these areas.

## ACKNOWLEDGMENTS

We are very appreciative of an anonymous reviewer for important comments. We wish to thank Dr. L. Floch and Dr. Yi-Ming Hu for their valuable suggestions. L.Q. would like to thank Mrs Ding Wei for her long-term support. This work is supported by the National Key R&D Program of China (Grant No. 2020YFC2200500) and the National Natural Science Foundation of China (Grants No. 12075325, No. 12005308, and No. 11605065).

- 
- [1] K. Danzmann and LISA Study Team, LISA: Laser interferometer space antenna for gravitational wave measurements, *Class. Quantum Gravity* **13**, A247 (1996).
  - [2] P. Amaro-Seoane, H. Audley, S. Babak, J. Baker, E. Barausse, P. Bender, E. Berti, P. Binetruy, M. Born, D. Bortoluzzi, *et al.*, Laser interferometer space antenna, [arXiv:1702.00786](https://arxiv.org/abs/1702.00786) (2017).
  - [3] Y. Gong, J. Luo, and B. Wang, Concepts and status of Chinese space gravitational wave detection projects, *Nat. Astron.* **5**, 881 (2021).
  - [4] J. Luo, L.-S. Chen, H.-Z. Duan, Y.-G. Gong, S. Hu, J. Ji, Q. Liu, J. Mei, V. Milyukov, M. Sazhin, *et al.*, TianQin: A space-borne gravitational wave detector, *Class. Quantum Gravity* **33**, 035010 (2016).
  - [5] J. Mei, Y.-Z. Bai, J. Bao, E. Barausse, L. Cai, E. Canuto, B. Cao, W.-M. Chen, Y. Chen, Y.-W. Ding, *et al.*, The TianQin project: Current progress on science and technology, *Prog. Theor. Exp. Phys.* **2021**, 05A107 (2021).
  - [6] W. Su, Y. Wang, Z.-B. Zhou, Y.-Z. Bai, Y. Guo, C. Zhou, T. Lee, M. Wang, M.-Y. Zhou, T. Shi, *et al.*, Analyses of residual accelerations for TianQin based on the global MHD simulation, *Class. Quantum Gravity* **37**, 185017 (2020).
  - [7] H. Yin, D.-Y. Tan, M. Hu, S. Wang, Y.-Z. Bai, S.-C. Wu, and Z.-B. Zhou, Measurements of Magnetic Properties of Kilogram-Level Test Masses for Gravitational-Wave Detection using a Torsion Pendulum, *Phys. Rev. Appl.* **15**, 014008 (2021).
  - [8] M. Diaz-Aguiló, Ph.D. thesis, Universitat Politècnica de Catalunya (UPC), 2011.
  - [9] M. Hueller, M. Armano, L. Carbone, A. Cavalleri, R. Dolesi, C. Hoyle, S. Vitale, and W. Weber, Measuring the LISA test mass magnetic properties with a torsion pendulum, *Class. Quantum Gravity* **22**, S521 (2005).
  - [10] M. Diaz-Aguiló, E. García-Berro, and A. Lobo, Inflight magnetic characterization of the test masses onboard LISA Pathfinder, *Phys. Rev. D* **85**, 042004 (2012).
  - [11] M. Armano, H. Audley, J. Baird, P. Binetruy, M. Born, D. Bortoluzzi, E. Castelli, A. Cavalleri, A. Cesarini, A. Cruise, *et al.*, Beyond the Required LISA Free-Fall Performance, New LISA Pathfinder Results down to 20  $\mu$ Hz, *Phys. Rev. Lett.* **120**, 061101 (2018).
  - [12] C. Prados, R. Del Real, D.-X. Chen, B.-Z. Li, and A. Hernando, Susceptibility spectrum of a magnetic conducting sphere, *Rev. Sci. Instrum.* **65**, 3044 (1994).
  - [13] C. Topping and S. Blundell, AC susceptibility as a probe of low-frequency magnetic dynamics, *J. Phys.: Condens. Matter* **31**, 013001 (2018).
  - [14] L. Zaragoza, Ph.D. thesis, Universitat autònoma de barcelona, 2020.
  - [15] F. Antonucci, M. Armano, H. Audley, G. Auger, M. Benedetti, P. Binetruy, C. Boatella, J. Bogenstahl, D. Bortoluzzi, P. Bosetti, *et al.*, From laboratory experiments to LISA Pathfinder: Achieving LISA geodesic motion, *Class. Quantum Gravity* **28**, 094002 (2011).
  - [16] N. R. Dilley, M. McElfresh, and A. C. Susceptometry, in *Magnetic Measurement Techniques for Materials Characterization* (Springer, Cham, 2021), p. 63.
  - [17] M. Armano, H. Audley, J. Baird, P. Binetruy, M. Born, D. Bortoluzzi, E. Castelli, A. Cavalleri, A. Cesarini, and A. M. Cruise, *et al.*, Spacecraft and interplanetary contributions to the magnetic environment on-board LISA Pathfinder, *Mon. Not. R. Astron. Soc.* **494**, 3014 (2020).
  - [18] L. Zhu, Q. Liu, H.-H. Zhao, S.-Q. Yang, P. Luo, C.-G. Shao, and J. Luo, Magnetic effect in the test of the weak equivalence principle using a rotating torsion pendulum, *Rev. Sci. Instrum.* **89**, 044501 (2018).
  - [19] G. Gillies and R. Ritter, Torsion balances, torsion pendulums, and related devices, *Rev. Sci. Instrum.* **64**, 283 (1993).
  - [20] Shanghai Goodstar Technology Co. Ltd. Copper: GS-CU39K20; Fused silica: GS-QZ39K20.
  - [21] J. C. Maxwell, *A Treatise on Electricity and Magnetism* (Clarendon Press, 1873), Vol. 1, pp. 333–334.
  - [22] D. Nicolodi, Ph.D. thesis, University of Trento, 2011.
  - [23] L. Zhu, Q. Liu, H.-H. Zhao, Q.-L. Gong, S.-Q. Yang, P. Luo, C.-G. Shao, Q.-L. Wang, L.-C. Tu, and J. Luo, Test of the Equivalence Principle with Chiral Masses using a Rotating Torsion Pendulum, *Phys. Rev. Lett.* **121**, 261101 (2018).
  - [24] G. L. Smith, C. D. Hoyle, J. H. Gundlach, E. G. Adelberger, B. R. Heckel, and H. E. Swanson, Short-range tests of the equivalence principle, *Phys. Rev. D* **61**, 022001 (1999).
  - [25] S. Vitale, M. Armano, L. Carbone, A. Cavalleri, G. Ciani, R. Dolesi, M. Hueller, D. Tombolato, and W. J. Weber, in *AIP Conference Proceedings* (American Institute of Physics, Greenbelt, 2006), Vol. 873, p. 507.
  - [26] K. H. Kiyani, K. T. Osman, and S. C. Chapman, Dissipation and heating in solar wind turbulence: From the macro to the micro and back again, *Philos. Trans. R. Soc. A* **373**, 20140155 (2015).
  - [27] J. J. Ho Zhang, Master's thesis, Universitat Politècnica de Catalunya, 2019.
  - [28] M. Jackson, Imaginary susceptibility, a primer, *IRM Quart.* **13**, 10 (2003).
  - [29] M. C. Wapler, J. Leupold, I. Dragonu, D. von Elverfeld, M. Zaitsev, and U. Wallrabe, Magnetic properties of materials for MR engineering, micro-MR and beyond, *J. Magn. Reson.* **242**, 233 (2014).
  - [30] C. E. Mullin, Magnetic susceptibility of the soil and its significance in soil science: A review, *J. Soil Sci.* **28**, 223 (1977).
  - [31] S. Y. Dan'kov, A. M. Tishin, V. K. Pecharsky, and K. A. Gschneidner, Magnetic phase transitions and the

- magnetothermal properties of gadolinium, *Phys. Rev. B* **57**, 3478 (1998).
- [32] H. Casimir and F. Du Pré, Note on the thermodynamic interpretation of paramagnetic relaxation phenomena, *Physica* **5**, 507 (1938).
- [33] D. C. Jiles and D. L. Atherton, Theory of ferromagnetic hysteresis, *J. Magn. Magn. Mater.* **61**, 48 (1986).
- [34] K. Binder and A. P. Young, Spin glasses: Experimental facts, theoretical concepts, and open questions, *Rev. Mod. Phys.* **58**, 801 (1986).